PREPARED FOR SUBMISSION TO JHEP

On-shell Approach to Anomalous Thresholds

Ting-Kai Hsu

Department of Physics and Center for Theoretical Physics, National Taiwan University, Taipei 10617, Taiwan

E-mail: b11901097@ntu.edu.tw

ABSTRACT: Positivity bounds on Wilson coefficients are typically derived from dispersion relations governed by normal (physical) threshold singularities. However, when the external particles possess finite widths, anomalous thresholds can enter the physical sheet through branch cuts, contributing to the dispersion relations. In this work, we develop an on-shell framework to systematically extract these contributions. In this approach, the anomalous thresholds are expressed entirely in terms of low-energy observables, without requiring any knowledge of the branch cut. Subtracting these contributions restores the standard positivity bounds.

Contents

1 Introduction

This document is a provisional research note summarizing the current status of an ongoing project. Its organization is as follows. Section 2 reviews the dispersion relation for stable and unstable kinematics. Section 3 provides an on-shell, IR computable approach for anomalous-threshold contribution, and we conclude that the positivity can be restored in the unstable region by subtracting this term. We dedicate the next section to an example of SMEFT and show the numerical result of the low-energy expansion coefficient B_2 in both stable and unstable regions. We then demonstrate the restoration of positivity in the unstable region by subtracting the anomalous-threshold contribution. All statements and results presented here are preliminary and subject to revision. Any remaining errors are solely the responsibility of the author.

2 Review of the Anomalous Threshold and the Double Discontinuity

In this section, we provide a brief review of the S-matrix for unstable particles, the anomalous threshold, and the double discontinuity in the dispersion relation.

Consider a scattering amplitude for a 2-to-2 elastic process. With $s = (p_1+p_2)^2$ and $t = (p_1 - p_4)^2$, for real kinematics, $(s > 0, t < 0)$ we will assume that,

- the amplitude $\mathcal{A}_4(s,t)$ is analytic in the upper-half s plane, and $\mathcal{A}_4(s,t) = \mathcal{A}_4^*(s^*,t)$,

- the amplitude is s–u symmetric, $\mathcal{A}_4(s,t) = \mathcal{A}_4(u,t)$,
- $\mathcal{A}_4(s,t)/s^2$ is convergent in the high energy limit, $\lim_{|s|\to\infty} \mathcal{A}_4(s,t)/s^2 = 0$, and
- the singularities are normal thresholds, accompanying branch cuts.[1]

With these assumptions, one can set up a twice-subtracted dispersion relation. Since the non-analyticity in the complex plane corresponds to physical thresholds, we have the identity,

$$\oint_C \frac{ds'}{2\pi i} \frac{\mathcal{A}_4(s', t \to 0)}{(s'-s_0)^3} = 0\,, \tag{2.1}$$

where the contour is illustrated in figure 1. Due to the amplitude being asymptotically bounded by s^2, the above identity then relates the second derivative of the amplitude at the subtraction point s_0 to the discontinuity along the s and u channel branch cuts. In particular,

$$B_2(s_0, s_i) \equiv \partial_s^2 \mathcal{A}_4(s)|_{s=s_0} = 2\int_{m^2_{\text{normal}}}^{\infty} \frac{ds'}{2\pi i} \frac{\text{Disc}_s \mathcal{A}_4(s')}{(s'-s_0)^3}, \tag{2.2}$$

where $s_i = p_i^2$ are masses of external particles, m^2_{normal} is the s-channel normal threshold, and $\mathcal{A}_4(s)$ the forward amplitude. Note that s_0 is chosen to be at the $s \leftrightarrow u$ crossing-symmetric point. Thus, after a change of variable, the integration along u-channel discontinuity will be the same as the s-channel and hence the factor of 2 on the RHS.

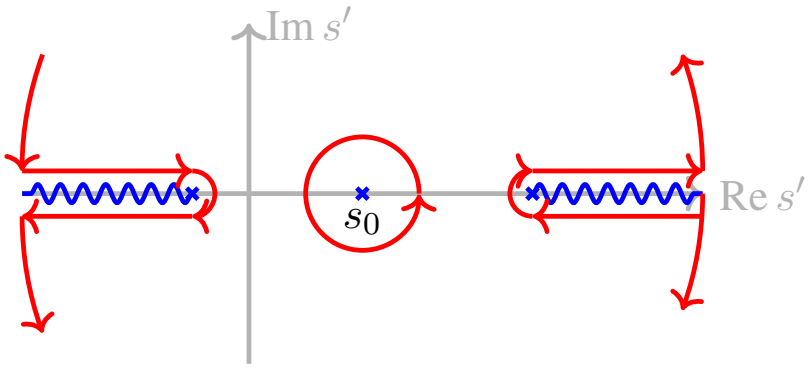

Figure 1: Integration contour for the dispersion relation, avoiding branch cuts and enclosing subtraction point s_0.

We will be interested in how the dispersion relation in eq.(2.2) can be modified when the external states are no longer the lightest state in the spectrum. In such a case, new contributions due to non-zero decay widths and anomalous thresholds introduce new non-analyticity on the physical sheet. To proceed, we first address how the S-matrix for unstable particles can be defined.

2.1 S-Matrix for Unstable Particles

First, let's recall the definition of the unstable particle in perturbation theory. Let $i\Sigma(p^2)$ be a one-particle-irreducible two-point function, which has a multi-particle branch point at $p^2 = m^2_{\text{th}}$

[1] Singularities are poles if they are associated with one-particle states.

with m_{th} being the sum of masses participating in the multi-particle production. Resuming the propagator corrections yield,

$$\frac{i}{p^2-m_b^2}+\frac{i}{p^2-m_b^2}\left(i\Sigma(p^2)\right)\frac{i}{p^2-m_b^2}+\cdots=\frac{i}{p^2-m_b^2-\Sigma(p^2)}\equiv\frac{i}{p^2-M^2(p)}\,,$$

where $\text{Re}M^2=m_b^2-\text{Re}\Sigma$ and $\text{Im}M^2=-i\text{Im}\Sigma$. When $p^2<m_{\text{th}}^2$, $\Sigma(p^2)$ is real and becomes complex when $p^2>m_{\text{th}}^2$. The resonance of the unstable pole is a Breit-Wigner distribution, where the decay width $\Gamma\equiv\text{Im}\Sigma/M_R$ is defined from the normalized width of the resonance

$$\left|\frac{i}{p^2-M^2}\right|^2=\frac{1}{(p^2-(m_b^2+\text{Re}\Sigma))^2+(\text{Im}\Sigma)^2}\equiv\frac{1}{(p^2-M_R^2)^2+M_R^2\Gamma^2}\tag{2.3}$$

From the optimal theorem, the imaginary part $\text{Im}\Sigma$ is positive. Because the unstable pole has a negative imaginary part, it is called a decaying mode. To reach such an unstable pole, p^2 has to cross the branch cut $p^2>m_{\text{th}}^2$ and analytically continue to the unphysical sheet in the causal $+i\epsilon$ direction, denoted by a plus sign $(+)$. See Figure 2 for illustration.

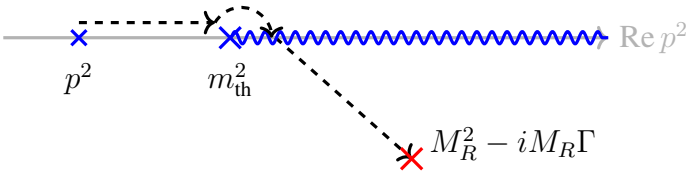

Figure 2: Decaying mode: p^2 analytically continues to the unstable pole at the lower-half plane in the $(i\epsilon)$ causal direction.

In general, we define the unstable particles as the poles on the second sheet of amplitudes. Utilizing the factorization at the unstable pole, the S-matrix with external unstable states can be defined by taking the residue of the scattering amplitudes of stable particles. In this paper, we are interested in the four-point amplitude with two external unstable states. To define it, consider the residue of a six-point diagram $\mathcal{A}_6(1,2',2'',3',3'',4)$ of stable particles (Fig. 3). Let $s_{2'2''}\equiv(p_{2'}+p_{2''})^2$ and $s_{3'3''}\equiv(p_{3'}+p_{3''})^2$ analytically continue $(++)$ to the unstable poles, M^2, and other kinematics are fixed, the residue of $\mathcal{A}_6$ factorizes into a product of three-point amplitudes and a four-point amplitude. The last one defines four-point amplitude with two external unstable states, $\mathcal{A}_4^{++}\equiv\mathcal{A}_4(s_{3'3''}^+,\,s_{2'2''}^+)$. In addition, by real analyticity, the six-point diagram possesses conjugate poles $(M^2)^*$ that can be reached by analytic continuation in the anti-causal $(-i\epsilon)$ direction, denoted by a minus sign $(-)$. In this paper, we focus on $\mathcal{A}_4^{+-}\equiv\mathcal{A}_4(s_{3'3''}^+,\,s_{2'2''}^-)$ and $\mathcal{A}_4^{++}$ since the other configurations can be obtained by complex conjugation.

We will work in perturbation theory. The Feynman rule gives the factorization structure

$$\begin{aligned}\mathcal{A}_6=&\,\mathcal{A}_3(s_{3'3''})\frac{1}{s_{3'3''}-M^2(s_{3'3''})}\mathcal{A}_4(s_{2'2''},s_{3'3''})\frac{1}{s_{2'2''}-M^2(s_{2'2''})}\mathcal{A}_3(s_{2'2''})\\&+(\text{terms without unstable-particle propagators})\end{aligned}\tag{2.4}$$

where $\mathcal{A}_3$ and $\mathcal{A}_4$ are off-shell three-point and four-point amplitudes. The residue is given by these off-shell amplitudes evaluated at the unstable poles. Hence, at least in perturbation theory, the

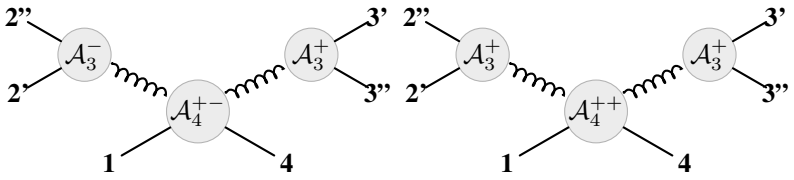

Figure 3: Six-point diagrams factorize into a four-point amplitude with two external unstable states and three-point amplitudes at the unstable poles.

computation of the unstable-particle amplitudes boils down to analytic continuation of the four-point amplitude in the external mass variables.

2.2 Triangle Branch Points and Double Discontinuity

Before moving to the problem of analytic continuation in external masses, let us discuss the analytic structure in the lightest particle scattering. In perturbation theory, the amplitude can have complicated branch points corresponding to multiple propagators going on-shell. However, most of these singularities do not live on the physical (principal) sheet when the external particles are lightest. That is, most of these singularities can only be reached by starting in the physical region and passing through branch cuts associated with standard particle production. For $2 \to 2$ amplitude at one-loop, these singularities are simple to track. The first branch point on the complex s plane is the two-particle normal threshold, m^2_{normal} corresponding to two propagators going on-shell. As s analytically continues across the associated branch cut, it enters the second sheet. In the second sheet, a new branch point would appear if another propagator goes on-shell, i.e. the triangle branch point $s_\triangleleft$. Continuing onward, one finds the box branch-point in the next sheet. This is illustrated in Figure 4.

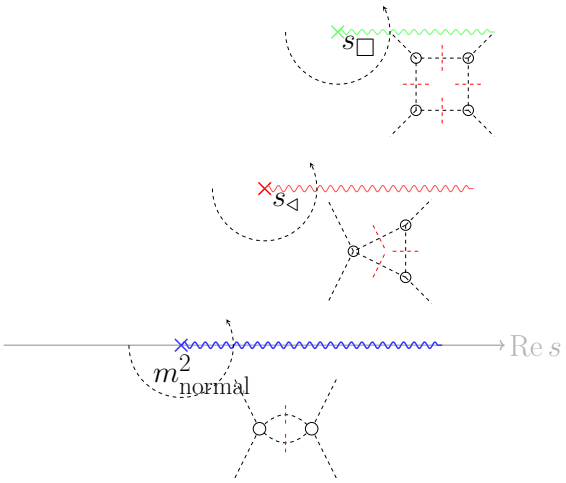

Figure 4: Analytic continuation across the branch cut to enter the higher sheet. We encounter the triangle singularity on the second sheet and then the box singularity on the third sheet.

We elaborate on this analytic structure more explicitly. We define the scalar box and triangle

integrals by

$$\mathcal{I}_4 = \int \frac{d^4L}{(2\pi)^4}\frac{1}{D_0D_1D_2D_3}, \quad \mathcal{I}_3^{\triangleright} = \int \frac{d^4L}{(2\pi)^4}\frac{1}{D_0D_1D_2}, \quad \mathcal{I}_3^{\triangleleft} = \int \frac{d^4L}{(2\pi)^4}\frac{1}{D_0D_2D_3}, \tag{2.5}$$

Here we assume all momenta are outgoing, so $D_0{=}L^2{-}m_0^2$, $D_1{=}(L{+}p_1)^2{-}m_1^2$, $D_2{=}(L{+}p_{12})^2{-}m_2^2$, and $D_3{=}(L{+}p_{123})^2{-}m_3^2$. They are the integrals relevant to s channel triangle and box singularities at one-loop level. The locations of singularities are determined by the Landau equations: (i) propagators go on-shell, and (ii) the zeros of on-shell propagators pinch the integration contour[2]. The second condition translates into the condition that $\det \mathbf{Q} = 0$, where $\mathbf{Q}_{ij} \equiv L_i \cdot L_j$ for $L_i \equiv L + \sum_{k=1}^{i} p_k$. We denote the determinant of each topology by

$$S_{\square} = \det \mathbf{Q} \quad \text{for} \quad D_0 = D_1 = D_2 = D_3 = 0\,, \tag{2.6}$$

$$S_{\triangleright} = \det \mathbf{Q} \quad \text{for} \quad D_0 = D_1 = D_2 = 0\,, \tag{2.7}$$

$$S_{\triangleleft} = \det \mathbf{Q} \quad \text{for} \quad D_0 = D_2 = D_3 = 0\,. \tag{2.8}$$

For instance, $\mathbf{Q}$ for $D_0 = D_1 = D_2$ is

$$\mathbf{Q} = \begin{pmatrix} m_0^2 & L\cdot L_1 & L\cdot L_2 \\ L\cdot L_1 & m_1^2 & L_1\cdot L_2 \\ L\cdot L_2 & L_1\cdot L_2 & m_2^2 \end{pmatrix}$$

and the solutions of $S_{\triangleright} = 0$ for s are

$$s_{\triangleright}^{\pm}(s_1, s_2) \equiv s_2 + s_1 + \frac{-(s_2 + m_1^2 - m_2^2)(s_1 + m_1^2 - m_0^2) \pm \sqrt{\lambda(s_2, m_1^2, m_2^2)\lambda(s_1, m_1^2, m_0^2)}}{2m_1^2} \tag{2.9}$$

where $\lambda(x, y, z) \equiv x^2 + y^2 + z^2 - 2(xy + yz + zx)$.

As we mentioned at the beginning, the triangle singularities $S_{\triangleright} = 0$ and $S_{\triangleleft} = 0$ are found on the second sheet, and the box ones $S_{\square} = 0$ are on the third sheet. They can be understood as follows. First, recall that when we analytically continue a complex function $f(z)$ through a branch cut, the functional form changes as

$$f(z) \to f(z) \pm \mathrm{Disc} f(z)\,, \tag{2.10}$$

where the sign depends on which side of the cut we continue from. Therefore, new singularities on the second sheet arise from the singularities of the discontinuity. For the one-loop integrals, applying the two-particle cut in s channel, the discontinuity across the normal threshold $m^2_{\text{normal}} = (m_2 + m_0)^2$ is

$$\frac{\mathrm{Disc}_s \mathcal{I}_3^{\triangleright}}{2\pi i} = \frac{1}{\sqrt{\lambda_{\triangleright}}} \log\left(\frac{\sqrt{2sS_{\triangleright} + \lambda_{s02}\lambda_{\triangleright}} - \sqrt{\lambda_{s02}\lambda_{\triangleright}}}{\sqrt{2sS_{\triangleright} + \lambda_{s02}\lambda_{\triangleright}} + \sqrt{\lambda_{s02}\lambda_{\triangleright}}}\right), \tag{2.11}$$

$$\frac{\mathrm{Disc}_s \mathcal{I}_4}{2\pi i} = \frac{1}{\sqrt{S_{\square}}} \log\left(\frac{\sqrt{S_{\triangleright}S_{\triangleleft} + \lambda_{s02}S_{\square}} + \sqrt{\lambda_{s02}S_{\square}}}{\sqrt{S_{\triangleright}S_{\triangleleft} + \lambda_{s02}S_{\square}} - \sqrt{\lambda_{s02}S_{\square}}}\right), \tag{2.12}$$

[2]Here the integration contour means the loop momentum integration.

where $\lambda_\triangleright \equiv \lambda(s, s_1, s_2)$, $\lambda_{s02} \equiv \lambda(s, m_0^2, m_2^2)$. The expression for $\triangleleft$ is obtained by replacing $\triangleleft \to \triangleright$ in (2.11) with $\lambda_\triangleleft \equiv \lambda(s, s_3, s_4)$. We see that the triangle branch points ($S_\triangleright = 0$, $S_\triangleleft = 0$) cause the argument of logarithms in $\text{Disc}_s\mathcal{I}_4$ and $\text{Disc}_s\mathcal{I}_3^\triangleright$ to approach 0 or infinity, yielding the branch cuts on the second sheet. On the other hand, (2.12) is not singular at $S_\square = 0$ as long as the logarithm takes the principal value, concluding no box singularity on the second sheet. The discontinuities at the triangle branch points are computed by the discontinuities of (2.11) and (2.12), namely the double discontinuities

$$\text{Disc}_s^2\mathcal{I}_4 = \frac{(2\pi i)^2}{\sqrt{S_\square}}, \qquad \text{Disc}_s^2\mathcal{I}_3^\triangleright = \frac{(2\pi i)^2}{\sqrt{\lambda_\triangleright}}. \tag{2.13}$$

One can see that the double discontinuity has the branch points at $S_\square = 0$, which generate the box singularities on the third sheet of $\mathcal{I}_4$.[3]

2.3 Anomalous Thresholds and Modified Dispersion Relations

The location of triangle branch points, Eq. (2.9), is a function of s_1, s_2. While the triangle branch points are on the second sheet for small s_1 and s_2, they can enter the physical sheet as the external masses increase. This new singularity on the physical sheet is referred to as the *anomalous threshold*, which modifies the dispersion relation accordingly.

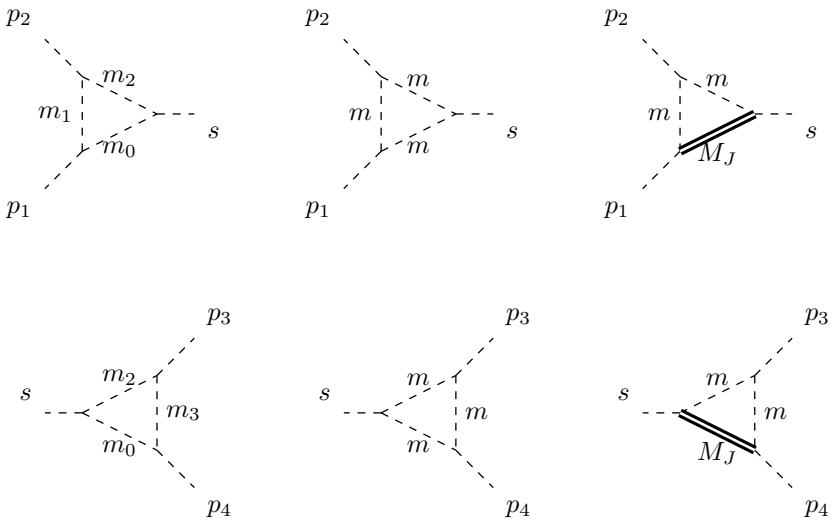

Figure 5: Left: A general one-loop triangle diagram. Middle: Triangle diagrams with external kinematics and integral masses being in the IR region. Right: Triangle diagrams with one of the internal masses being in the UV region.

We begin with the case where all parameters are in the IR. For example, let $m_0 = m_1 = m_2 = m$ and $s_1 = s_2 = p^2$, corresponding to the middle of Fig. 5. The triangle branch points and the two-particle normal threshold are then

$$s_\triangleright^\pm(p^2) = \left(0, 4p^2 - \frac{p^4}{m^2}\right), \quad m^2_{\text{normal}} = 4m^2.$$

[3] $\lambda_\triangleright = 0$ is known as a non-Landauian or second type singularity.

As p^2 approaches $2m^2$, one of the triangle branch points, $s_\triangleright^+$, approaches the two-particle normal threshold from below; adding a small imaginary part to detour $p^2 = 2m^2$, $s_\triangleright^+$ encircles the two-particle normal threshold, entering the physical sheet as $p^2 > 2m^2$ (Fig. 6 left). In this case, the anomalous threshold can be present even when the external kinematic p^2 is below the decay threshold, $2m^2 < p^2 < 4m^2$. If the external kinematics p^2 further increase to $p^2 > 4m^2$, we obtain the anomalous threshold for unstable kinematics. The position of $s_\triangleright^+$ depends on whether s_1 and s_2 are continued to the decaying modes or the growing modes, see [1] for more details.

Figure 6: Left: One of the triangle branch points enters the physical sheet by encircling the two-particle normal threshold, indicated by the red line. Right: The contour of dispersive integration is deformed, which can be written into two pieces: the anomalous-threshold contribution from $s_\triangleright^+$ to $4m^2$ and the normal threshold contribution from $4m^2$ to infinity.

Through the analytic continuation, the contour of the dispersive integral (2.2) is deformed as illustrated in the middle panel of Fig. 6. The integration contour below the normal threshold goes around the anomalous threshold and returns to the normal threshold. This integral can be rewritten as the integral of the double discontinuity, which precisely represents the dispersive integral along the anomalous cut $s_\triangleright < s < 4m^2$. The modified dispersion relation is thus [2]

$$B_2 = 2\int_{4m^2}^{\infty} \frac{ds'}{2\pi i} \frac{\text{Disc}_s\, \mathcal{A}_4(s')}{(s'-s_0)^3} + 2\sum_\sigma \int_{s_\sigma^+}^{4m^2} \frac{ds'}{2\pi i} \frac{\text{Disc}_s^2\, \mathcal{A}_4(s')}{(s'-s_0)^3}\,, \tag{2.14}$$

where $\sigma = \triangleleft, \triangleright$. The dispersion relation clearly disentangles the normal and anomalous contributions to the low-energy coefficient B_2:

$$B_{2,\text{norm}} \equiv 2\sum_\sigma \int_{s_+}^{4m^2} \frac{ds'}{2\pi i} \frac{\text{Disc}_s\, \mathcal{A}_4(s')}{(s'-s_0)^3}\,, \tag{2.15}$$

$$B_{2,\text{IR, anom}} \equiv 2\sum_\sigma \int_{s_\sigma^+}^{4m^2} \frac{ds'}{2\pi i} \frac{\text{Disc}_s^2\, \mathcal{A}_4(s')}{(s'-s_0)^3}\,. \tag{2.16}$$

In this case, the anomalous threshold is in IR, so the anomalous-threshold contribution (2.16) is IR-computable. Hence, we can compute $B_2 - B_{2,\text{IR, anom}} = B_{2,\text{norm}}$ within a low-energy theory, and obtain the positivity bound on the low-energy observable $B_2 - B_{2,\text{IR, anom}} > 0$ from the positivity of the normal threshold cut.

Let's now turn to the case where one of the internal masses is in the UV region (Fig. 5 right), $m_0^2 = M_J^2 \gg s_1,\, s_2,\, m_1^2 = m_2^2 = m^2$. We analytically continue s_2 for a fixed small s_1, as shown in Fig. 7a. The triangle branch points and the two-particle normal threshold are

$$s_\triangleright^\pm(s_2) = \frac{M_J^2}{2m^2}\left(s_2 \pm \sqrt{s_2(s_2-4m^2)}\right) + \mathcal{O}(1/M_J^2), \quad m^2_{\text{normal}} = (m+M_J)^2\,, \tag{2.17}$$

where we have performed a large M_J expansion in the former. In $s_2 < m^2_{\text{th}} = 4m^2$, the triangle branch points are on the second sheet (Fig. 7b). As s_2 approaches the decay threshold $m^2_{\text{th}} = 4m^2$,

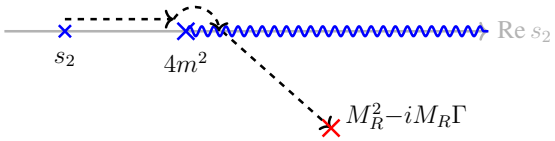

(a) Analytic continuation (decaying mode, denoted by $+$) of s_2 toward the unstable pole $M_R^2 - iM_R\Gamma$ in the complex plane.

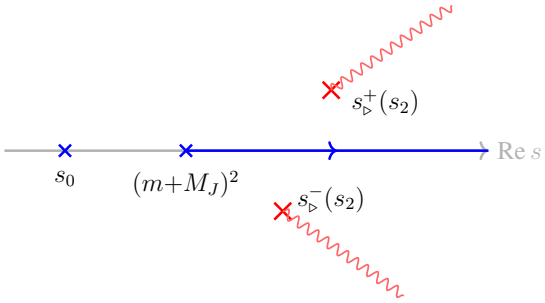

(b) The triangle branch points $s_\triangleright^\pm(s_2)$ are on the unphysical sheet for $s_2 < 4m^2$. This corresponds to the section 1 in Fig. 7a.

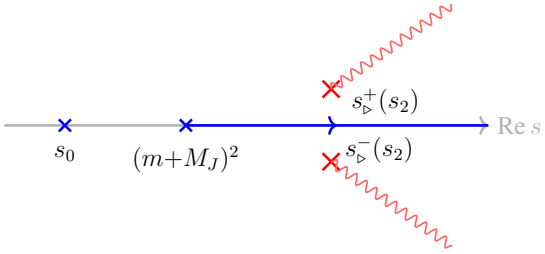

(c) The triangle branch points $s_\triangleright^\pm(s_2)$ become degenerate near the decay threshold $\mathrm{Re}(s_2) = 4m^2$. This corresponds to the section 2 in Fig. 7a.

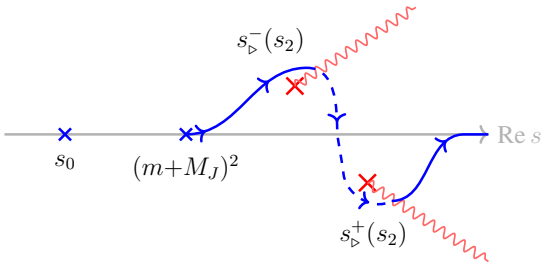

(d) The triangle branch points $s_\triangleright^\pm(s_2)$ enter the physical sheet in the complex s plane as the external variable s_2 is analytically continued to the unstable pole. This corresponds to the section 3 in Fig. 7a.

Figure 7: Fig. 7a illustrates the analytical continuation of the external kinematic variable s_2 to the unstable pole, delineated by three distinct sections. The corresponding trajectories of the triangle branch points $s_\triangleright^\pm(s_2)$ for each section are depicted in Fig. 7b, 7c, and 7d, respectively.

the triangle branch points are degenerate (Fig. 7c), $s_\triangleright^\pm = 2M_J^2$. When s_2 analytically continues into the unstable region, the triangle branch points cross the normal threshold cut, entering the physical sheet (Fig. 7d). This anomalous threshold is in UV, $s_\triangleright^\pm = \mathcal{O}(M_J^2)$, and appears in the physical sheet only if the external kinematics are unstable.

The contour deformation of the dispersion relation is also shown in Fig. 7. In Fig. 7d, the branch cuts (the red wavy lines) are refined so that the deformed contour passes through one branch cut onto the second sheet and then returns through the second branch cut. The integral can then be divided into two pieces: the first integration runs along the real axis in the physical sheet, and the second one is a closed path connecting the pair of triangle branch points:

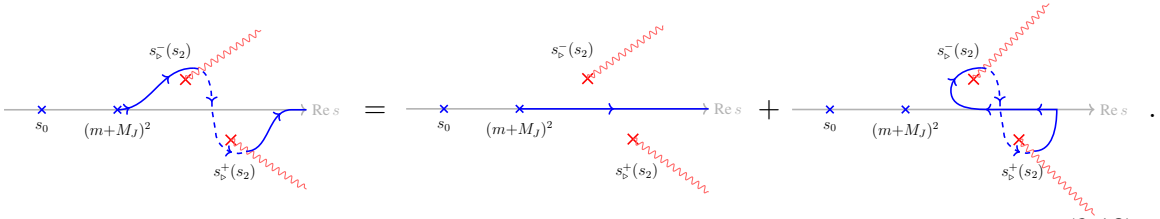

(2.18)

The second integral can be recast as the integral of the double discontinuity, yielding the dispersion

relation [1]

$$B_2^{+-} = 2\int_{(m+M_J^2)}^{\infty} \frac{ds'}{2\pi i} \frac{\text{Disc}_s\left(\mathcal{A}_4^{+-}(s')\right)}{(s'-s_0)^3} + 2\sum_{\sigma}\int_{s_\sigma^+}^{s_\sigma^-} \frac{ds'}{2\pi i} \frac{\text{Disc}_s^2\left(\mathcal{A}_4^{+-}(s')\right)}{(s'-s_0)^3}\,. \tag{2.19}$$

Here, $+-$ denotes the direction of the analytic continuation of the external mass variables s_2 and s_3. We again define the normal and anomalous contributions as

$$B_{2,\text{norm}}^{+-} \equiv 2\int_{(m+M_J^2)}^{\infty} \frac{ds'}{2\pi i} \frac{\text{Disc}_s\left(\mathcal{A}_4^{+-}(s')\right)}{(s'-s_0)^3}\,, \tag{2.20}$$

$$B_{2,\text{UV anom}}^{+-} \equiv 2\sum_{\sigma}\int_{s_\sigma^+}^{s_\sigma^-} \frac{ds'}{2\pi i} \frac{\text{Disc}_s^2\left(\mathcal{A}_4^{+-}(s')\right)}{(s'-s_0)^3}\,. \tag{2.21}$$

With the conjugate choice $s_3{=}s_2^*$, the positivity of (2.20) is ensured by unitarity [3]. However, unlike the previous case, the anomalous thresholds $s_\sigma^\pm$ lie in the UV region, and as such cannot be calculated in a low-energy theory. It poses a problem to find an IR-computable positive quantity [1].

3 On-shell Approach to Anomalous-Threshold Contribution

From the previous section, we've seen that when considering unstable external states, the triangle branch points can enter the physical sheet by crossing the UV branch cut, which indicates that the anomalous-threshold contribution, Eq. (2.21), depends on the details of UV and is no longer IR-computable. However, in the explicit computations in [1], the loop amplitudes was computed using method of regions, where the loop momenta L is separated into the hard ($|L| \approx M_J$) and soft region ($|L| \ll M_J$). It was observed that the leading (in $1/M_J$) contribution to the anomalous threshold comes solely from the soft region. This hints at the possibility that the contributions can be captured by the Wilson coefficients of the low-energy EFT operators, and hence "IR measurable".

To fully render the UV anomalous threshold into an IR-computable contribution, we need to demonstrate that the way in which the anomalous threshold depends on the UV information, is such that it can be repackaged into IR-observables, i.e. the Wilson-coefficients. In this section, we will demonstrate that this iss indeed the case for the simple scenario where the UV d.o.f only couples to stable particles which are scalars. We will comment on more general case in the end.

3.1 Double Discontinuities Computed by Unitary Cuts

In four dimensions, the one-loop four-point amplitude can be decomposed into a sum of scalar integral basis:

$$\mathcal{A}_4 = d\,\mathcal{I}_4 + \sum_{\{i\}} c_{\{i\}}\,\mathcal{I}_3^{\{i\}} + \sum_{\{j\}} b_{\{j\}}\,\mathcal{I}_2^{\{j\}} + \sum_{\{k\}} a_{\{k\}}\,\mathcal{I}_1^{\{k\}} + R \tag{3.1}$$

Where the scalar box $\mathcal{I}_4$ is defined in Eq. (2.5) and $\{i\}$ in $I_n^{\{i\}}$ denotes appropriate subsets of n propagators D_i, i.e. scalar triangle, bubble, and tadpole integrals. R is the rational part and d, $c_{\{i\}}$, $b_{\{j\}}$, $a_{\{k\}}$ are integral coefficients. As we will be interested in the double discontinuity, we

will be only interested in $\mathcal{I}_4^{\{i\}}$, $\mathcal{I}_3^{\{i\}}$. These box and triangle-coefficients can be obtained from the generalized cut method [4]. If the integral coefficients are rational, then the double discontinuity of the amplitude is simply,

$$\begin{aligned}\text{Disc}_s^2\mathcal{A}_4 &= d\,\text{Disc}_s^2\,\mathcal{I}_4 + c_\triangleright\,\text{Disc}_s^2\,\mathcal{I}_3^\triangleright + c_\triangleleft\,\text{Disc}_s^2\,\mathcal{I}_3^\triangleleft \\ &= (2\pi i)^2\left(\frac{d}{\sqrt{S_\square}} + \frac{c_\triangleright}{\sqrt{\lambda_\triangleright}} + \frac{c_\triangleleft}{\sqrt{\lambda_\triangleleft}}\right).\end{aligned} \tag{3.2}$$

Where $\triangleleft$ and $\triangleright$ denote the left and right triangle introduced in Fig. 5 left.

Let us now review in detail how the integral coefficients are computed via generalized unitarity methods [5–7], verifying that they are in general rational. While this is obvious from the point of view of the Passarino-Veltman reduction formula [8], it is instructive to review the unitarity cut method so that when applied to the UV four-point amplitude, we will be able to track how the UV data is encoded in the integral coefficients.

The integral coefficients can be determined by applying cuts on both sides of Eq. (3.1). On the L.H.S., the result is given by the product of on-shell tree-amplitudes, with the momenta of the propagator satisfying the cut conditions. It will be convenient to parameterize the loop momentum as

$$L^\mu = \alpha q_1^\mu + \beta q_2^\mu + \frac{\gamma}{z}q^\mu + z\bar{q}^\mu \tag{3.3}$$

where we've introduced two null vectors, $q_1 \equiv \tilde{\lambda}_1\lambda_1$, $q_2 \equiv \tilde{\lambda}_2\lambda_2$, where $p_1{=}q_1{+}xq_2$, $p_2{=}q_2{+}yq_1$.[4] The orthogonal directions are then spanned by $q \equiv \tilde{\lambda}_1\lambda_2$, $\bar{q} \equiv \tilde{\lambda}_2\lambda_1$. Note that for the triple cut $(L{+}p_{12})^2{-}m_1^2{=}(L{+}p_{123})^2{-}m_2^2{=}L^2{-}m_0^2{=}0$, the parametrization of loop momentum is different: $L^\mu{=}\alpha' q_3^\mu{+}\beta' q_4^\mu{+}\frac{\gamma'}{z}q^\mu{+}z\bar{q}$, where $q_3{=}\tilde{\lambda}_3\lambda_3$, $q_4{=}\tilde{\lambda}_4\lambda_4$, and $q{=}\tilde{\lambda}_3\lambda_4$, $\bar{q}{=}\tilde{\lambda}_4\lambda_3$. Since we are interested in the box and triangle coefficient, we first begin with the triple cut, say $L^2{-}m_0^2{=}0$, $(L{+}p_1)^2{-}m_1^2{=}0$, $(L{+}p_{12})^2{-}m_2^2{=}0$. In this parametrization, the triple cut condition becomes a set of linear equations for α, β, γ, and thus they are just rational functions of external kinematics. The L.H.S. is the product of three amplitudes, where the summation over the internal states is implicit. If we further consider the quadruple cut, the final cut condition is a quadratic equation in z and hence the two solutions, denoted as $z_\pm$, have square-roots.

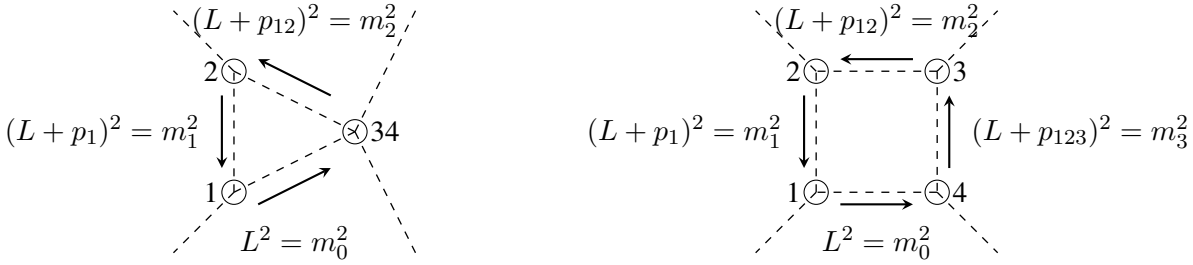

Quadruple cuts, given by the product of four tree amplitudes evaluated on the cut solutions, are used to determine the box coefficients. In particular, the box coefficient is given as:

$$d{=}\frac{\mathcal{A}_3^1\mathcal{A}_3^2\mathcal{A}_3^3\mathcal{A}_3^4(z_+){+}\mathcal{A}_3^1\mathcal{A}_3^2\mathcal{A}_3^3\mathcal{A}_3^4(z_-)}{2}. \tag{3.4}$$

[4] x and y can be solved by $p_2^2{=}s_1$, $p_2^2{=}s_2$, $(p_1{+}p_2)^2{=}s$

As one sums over the solutions z_+ and z_-, there are no square roots. The triangle coefficient can be obtained by differencing the residues at $z{=}\infty$ and $z{=}0$,

$$\begin{aligned} c_{\triangleright}&{=}\Big(\operatorname*{Res}_{z=\infty}-\operatorname*{Res}_{z=0}\Big)\,\frac{\mathcal{A}_3^1\mathcal{A}_3^2\mathcal{A}_4^{34}(z)}{2z},\ \text{ for triple cut } (L{+}p_1)^2{-}m_1^2{=}(L{+}p_{12})^2{-}m_2^2{=}L^2{-}m_0^2{=}0\\ c_{\triangleleft}&{=}\Big(\operatorname*{Res}_{z=\infty}-\operatorname*{Res}_{z=0}\Big)\,\frac{\mathcal{A}_3^3\mathcal{A}_3^4\mathcal{A}_4^{12}(z)}{2z},\ \text{ for triple cut } (L{+}p_{12})^2{-}m_2^2{=}(L{+}p_{123})^2{-}m_3^2{=}L^2{-}m_0^2{=}0. \end{aligned} \tag{3.5}$$

As one can see, no square roots are present.

3.2 Setup: UV Model

To illustrate the general procedure, we consider a simplified UV model with the following properties: (i) the UV state couples only to stable IR states in the loop, and (ii) all IR states are scalars while the UV state carries integer spin. This represents the simplest construction where the UV dynamics can be isolated through unitarity cuts, as external states coupling to the UV state (states 1 and 4) are separated from purely IR interactions (states 2 and 3). Consider a four-point amplitude with external states labeled by momenta p_i ($i{=}1,2,3,4$). The one-loop amplitude can be expanded on the scalar integral basis:

$$\mathcal{A}_4(p_1,p_2,p_3,p_4){=}$$

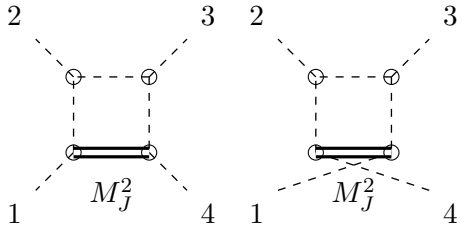

$$=\sum_{J=0}^{\infty}\int_{\Lambda^2}^{\infty}dM_J^2\delta_J(M_J^2)\left(d^J\mathcal{I}_4{+}c_{\triangleright}^J\mathcal{I}_3^{\triangleright}{+}c_{\triangleleft}^J\mathcal{I}_3^{\triangleleft}{+}\cdots\right){+}(s{\leftrightarrow}u). \tag{3.6}$$

Here $\cdots$ represents other scalar integrals, and Λ^2 is the EFT cutoff and $\delta_J(M_J^2)$ is a distribution indicating the positions of UV-states with spin J and mass M_J. The UV physics enters through: (i) the mass distribution $\delta_J(M_J^2)$, which for a single particle of mass M and spin j, reduces to $\delta_{J,j}\delta(M_J^2{-}M^2)$, and (ii) the integral coefficients (d^J, $c_{\triangleleft}^J$, $c_{\triangleright}^J$, and others). To determine these integral coefficients, we employ the generalized unitarity method. For the quadruple cut, let the three-point tree amplitudes attached to the cut propagators be

$$\begin{aligned} &\mathcal{A}^1\equiv\mathcal{A}(p_1,-L_1,L),\quad \mathcal{A}^2\equiv\mathcal{A}(L_1,p_2,-L_2),\\ &\mathcal{A}^3\equiv\mathcal{A}(L_2,p_3,-L_3),\quad \mathcal{A}^4\equiv\mathcal{A}(L_3,p_4,-L). \end{aligned} \tag{3.7}$$

The crucial feature is that only $\mathcal{A}^1$ and $\mathcal{A}^4$ involve the UV state (labeled by loop momentum L with spin J), while $\mathcal{A}^2$ and $\mathcal{A}^3$ couple purely IR states. This separation will be essential for the large M_J expansion and repackaging the UV information in terms of Wilson coefficients.

For the triple cuts, one of the internal IR states merges into a four-point amplitude:

$$\mathcal{A}^{12}\equiv\mathcal{A}(p_1,p_2,-L_2,L),\quad \mathcal{A}^{34}\equiv\mathcal{A}(L_2,p_3,p_4,-L). \tag{3.8}$$

Our assumption that internal IR states are scalars has a powerful consequence: the four-point amplitudes $\mathcal{A}^{12}$ and $\mathcal{A}^{34}$ in the triangle coefficients contain no polynomial terms, and they equal to the residues at the IR mass m^2

$$\mathcal{A}^{12}=\frac{\mathcal{A}^1\mathcal{A}^2}{L_1^2-m^2}, \quad \mathcal{A}^{34}=\frac{\mathcal{A}^3\mathcal{A}^4}{L_3^2-m^2}. \tag{3.9}$$

This factorization simplifies the formula for the triangle coefficients to products of three-point amplitudes only, which can be expressed in terms of the product of three-point tree amplitudes. Without this property (e.g., for spin-1 IR state exchange), additional polynomial terms would complicate the analysis. Therefore, we can evaluate the integral coefficients in terms of the product of three-point tree amplitudes. Let the product of three-point tree amplitudes

$$\text{For } \triangleright \text{ cut}, \quad f_J(z)\equiv\mathcal{A}^1\mathcal{A}^2\mathcal{A}^3\mathcal{A}^4(z); \quad \text{for } \triangleleft \text{ cut}, \quad g_J(z)\equiv\mathcal{A}^1\mathcal{A}^2\mathcal{A}^3\mathcal{A}^4(z). \tag{3.10}$$

and the integral coefficients

$$\begin{gathered} d^J=\frac{f_J(z_+)+f_J(z_-)}{2}, \\ c_{\triangleright}^J=\left(\operatorname*{Res}_{z=0}-\operatorname*{Res}_{z=\infty}\right)\frac{f_J(z)}{2z}, \quad c_{\triangleleft}^J=\left(\operatorname*{Res}_{z=0}-\operatorname*{Res}_{z=\infty}\right)\frac{g_J(z)}{2z} \end{gathered} \tag{3.11}$$

We adopt the convention to evaluate the box coefficient with the loop momentum parametrization in the $\triangleright$ triple-cut, in which it can be expressed in terms of $f_J(z)$.

Having established the cut expressions for the integral coefficients, the anomalous-threshold contribution can be rewritten as

$$\begin{aligned} B_{2,\text{UV anom}}^{+-}&=2\sum_\sigma\int_{s_\sigma^+}^{s_\sigma^-}\frac{ds'}{2\pi i}\frac{\text{Disc}_s^2\mathcal{A}_4^{+-}(s)}{(s'-s_0)^3} \\ &=2\sum_{J=0}^{\infty}\int_{\Lambda^2}^{\infty}dM_J^2\left[\left(\int_{s_\triangleright^+}^{s_\triangleright^-}+\int_{s_\triangleleft^+}^{s_\triangleleft^-}\right)\frac{ds'}{2\pi i}\frac{d^J\text{Disc}_s^2\mathcal{I}_4}{(s'-s_0)^3}+\int_{s_\triangleright^+}^{s_\triangleright^-}\frac{ds'}{2\pi i}\frac{c_\triangleright^J\text{Disc}_s^2\mathcal{I}_3^\triangleright}{(s'-s_0)^3}\right. \\ &\qquad\left.+\int_{s_\triangleleft^+}^{s_\triangleleft^-}\frac{ds'}{2\pi i}\frac{c_\triangleleft^J\text{Disc}_s^2\mathcal{I}_3^\triangleleft}{(s'-s_0)^3}\right] \end{aligned} \tag{3.12}$$

Since $M_J^2\gg s_0, s_i, m^2$, we could expand the anomalous-threshold contribution in powers of $1/M_J$ and take *the leading order*. The M_J dependence comes from three places: (i) the dispersion integration measure, (ii) the double discontinuity of the scalar integrals, and (iii) the integral coefficients. First, we isolate the M_J dependence in the integration measure by introducing the dimensionless variables $\zeta\equiv s'/M_J^2$. Under this change of variables, the integration bounds become:

$$\zeta_\sigma^\pm(s_i)=\frac{s_\sigma^\pm(s_i)}{M_J^2}=\frac{s_i\pm\sqrt{s_i(s_i-4m^2)}}{2m^2}+\mathcal{O}(M_J^{-4}), \tag{3.13}$$

which are M_J-independent at leading order and for $\sigma=\triangleright$, $s_i=s_2$; for $\sigma=\triangleleft$, $s_i=s_3$. Since $s_0/M_J^2\ll 1$, the dispersive integration becomes

$$\int_{s_\sigma^+}^{s_\sigma^-}\frac{ds'}{(s'-s_0)^3}=M_J^{-4}\int_{\zeta_\sigma^+}^{\zeta_\sigma^-}\frac{d\zeta}{\zeta^3}+\mathcal{O}\left(M_J^{-6}\right). \tag{3.14}$$

On the other hand, the double discontinuity of the amplitude factorizes into the integral coefficient and the double discontinuities of scalar integrals. Under the forward limit, for the double discontinuities of the scalar box and triangles, the leading terms are

$$\frac{1}{\sqrt{\lambda_{\triangleright}(s')}}=\frac{1}{M_J^2\zeta}+\mathcal{O}(M_J^{-4}),\ \ \frac{1}{\sqrt{\lambda_{\triangleleft}(s')}}=\frac{1}{M_J^2\zeta}+\mathcal{O}(M_J^{-4}),\ \ \frac{1}{\sqrt{S_{\square}(M_J^2)}}=\frac{1}{M_J^2(s_2-s_3)}+\mathcal{O}(M_J^{-4}).$$

While the M_J dependence of the integral coefficients arises from three sources: the three-point tree amplitudes, the cut solutions, and the integral variable s'. By mass-dimension analysis, a three-point amplitude in $4d$ should have one mass-dimension, which determines the leading scaling of the amplitude product in the large M_J expansion

$$f_J(z)=M_J^2 f_J^{(2)}(z)+\mathcal{O}\left(M_J\right),\quad g_J(z)=M_J^2 g_J^{(2)}(z)+\mathcal{O}\left(M_J\right). \tag{3.15}$$

where $f_J^{(2)}, g_J^{(2)}$ denotes the leading order of the expansion. Using the loop-momentum parametrization for the $\triangleright$ triple-cut, the leading terms of the quadruple-cut solutions scale as

$$z_{\pm}=\frac{s_2-s_3+t(1-\zeta)\pm\sqrt{(s_2-s_3+t(1-\zeta))^2-16\gamma\zeta^2\bar{q}\cdot p_3 q\cdot p_3}}{4\zeta\bar{q}\cdot p_3}+\mathcal{O}\left(M_J^{-2}\right). \tag{3.16}$$

Where $q=\tilde{\lambda}_1\lambda_2$, $\bar{q}=\tilde{\lambda}_2\lambda_1$, with γ fixed by the cut conditions, and we denote the leading term as $z_{\pm}^0$. Consequently, substituting $z_{\pm}^0$ into the amplitude preserves the M_J scaling of $f_J^{(2)}(z,\ell_i)$. The leading-order box coefficient in the large M_J expansion takes the form

$$d^J=M_J^2\frac{f_J^{(2)}(z_+^0)+f_J^{(2)}(z_-^0)}{2}+\mathcal{O}\left(M_J^0\right). \tag{3.17}$$

For the triangle coefficients, consider the Laurent series for $f_J^{(2)}(z), g_J^{(2)}(z)$

$$f_J^{(2)}(z)=\cdots+f_{-1}/z+f_J^0+f_1 z+\cdots,\quad g_J^{(2)}(z)=\cdots+g_{-1}/z+g_0+g_1 z+\cdots,$$

the triangle coefficients then take the form

$$c_{\triangleright}^J=M_J^2\left(\frac{f_{-1}}{4\gamma q\cdot p_3}+\frac{f_1}{4\bar{q}\cdot p_3}\right)+\mathcal{O}\left(M_J^0\right),\quad c_{\triangleleft}^J=M_J^2\left(\frac{g_{-1}}{4\gamma' q'\cdot p_1}+\frac{g_1}{4\bar{q}'\cdot p_1}\right)+\mathcal{O}\left(M_J^0\right). \tag{3.18}$$

Where $q'=\tilde{\lambda}_3\lambda_4$, $\bar{q}'=\tilde{\lambda}_4\lambda_3$, with γ' fixed by the $\triangleleft$ triple-cut condition. Combining these coefficient expansions with the double discontinuity of the scalar box and triangle integrals in the large M_J expansion, we obtain the leading anomalous-threshold contribution as

$$\begin{aligned}\Delta B_{2,\text{UV anom}}^{+-}=4\pi i\sum_{J=0}^{\infty}\int_{\Lambda^2}^{\infty}\frac{dM_J^2\delta_J(M_J^2)}{M_J^4}\Bigg[&\left(\int_{\zeta_{\triangleright}^+}^{\zeta_{\triangleright}^-}+\int_{\zeta_{\triangleleft}^+}^{\zeta_{\triangleleft}^-}\right)\frac{d\zeta}{\zeta^3}\frac{\left(f_J^{(2)}(z_+^0)+f_J^{(2)}(z_-^0)\right)}{2(s_2-s_3)}\\&+\int_{\zeta_{\triangleright}^+}^{\zeta_{\triangleright}^-}\frac{d\zeta}{\zeta^4}\left(\frac{f_{-1}}{4\gamma q\cdot p_3}+\frac{f_1}{4\bar{q}\cdot p_3}\right)+\int_{\zeta_{\triangleleft}^+}^{\zeta_{\triangleleft}^-}\frac{d\zeta}{\zeta^4}\left(\frac{g_{-1}}{4\gamma' q'\cdot p_1}+\frac{g_1}{4\bar{q}'\cdot p_1}\right)+\mathcal{O}\left(M_J^{-6}\right)\Bigg]\end{aligned} \tag{3.19}$$

In the large M_J expansion, we found that, at the leading order, the dispersion integration can be rescaled to be independent of M_J. This finding implies that we can exchange the order of the integral against the UV spectrum and the dispersion integration. Performing the integral against the UV spectrum before the dispersion integration packages the unknown UV information, indicating that the anomalous-threshold contribution can be expressed in terms of Wilson coefficients.

3.3 UV to IR-computable anomalous-threshold contribution

The unknown UV information is hidden in two places: (i) the distribution function of the UV states, $\delta_J(M_J^2)$, and (ii) the three-point amplitudes coupling to the UV states. Recall our assumption that the UV state only couples to stable IR states (including external states 1 and 4). Consider the four-point tree amplitude, and because of

$$\mathcal{B}_4(p_1,p_{1'},p_{4'},p_4)= \tag{3.20}$$

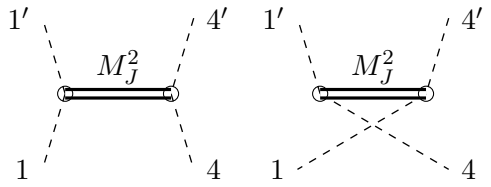

Because of the angular-momentum conservation, we can expand the full amplitude into a sum of partial-wave amplitudes $b_J(s_{11'})$ labeled by spin J

$$\mathcal{B}_4(p_1,p_{1'},p_{4'},p_4)=\sum_{J=0}^{\infty}16\pi(2J+1)b_J(s_{11'})\mathcal{P}_J\left(1+\frac{2t}{s_{11'}-4\mu^2}\right). \tag{3.21}$$

Here $\mathcal{P}_J\left(1+2t/(s_{11'}-4\mu^2)\right)$ is the Legendre polynomial, and $4\mu^2\equiv s_1+s_{1'}+s_{4'}+s_4$ and $s_{11'}\equiv(p_1+p_{1'})^2$. On the other hand, for low-energy condition $M_J^2>s_i,s,t$ ($i=1,1',4',4$, let the low-energy expansion of the amplitude

$$\mathcal{B}_4^{\text{low}}(s,t)=C_0+C_1t+C_2(s^2+u^2)+C_2't^2+\mathcal{O}(st) \tag{3.22}$$

Here $u=4\mu^2-s-t$. Consider a twice-subtracted dispersive sum rule with the following contour 9

$$I=\oint\frac{d\omega}{2\pi i}\frac{\mathcal{B}_4(\omega,t)}{(\omega-s_{11'})(\omega-s_0)^2}$$

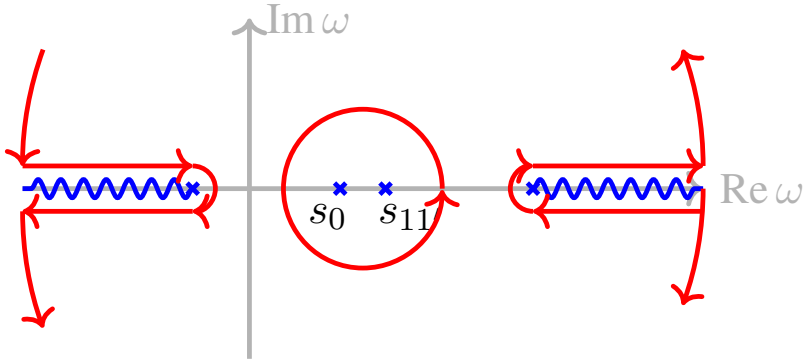

Figure 9: Integration contour for the dispersive sum rules, avoiding branch cuts and enclosing subtraction points: $s_0=(4\mu^2+t)/2$ and $s_{11'}$.

The contour reduces to two pieces: (i) the discontinuity contours along the s and u channel branch-cut and (ii) the residue at the IR-subtraction points $s_{11'}$ and s_0. The latter can be approxi-

mated by the low-energy expansion in Eq. (3.22).

$$\begin{aligned}&\frac{\mathcal{B}_4^{\text{low}}(s_{11'},t)}{(s_{11'}-s_0)^2}+\operatorname*{Res}_{\omega=s_0}\left(\frac{1}{\omega-s_{11'}}\frac{\mathcal{B}_4^{\text{low}}(\omega,t)}{(\omega-s_0)^2}\right)\\ =&16\sum_{J=0}^{\infty}\int_{\Lambda^2}^{\infty}d\omega\frac{(2J+1)\rho_J(\omega)\mathcal{P}_J\big(1+2t/(\omega-4\mu^2)\big)}{(\omega-s_0)^2}\left(\frac{1}{\omega-s_{11'}}+\frac{1}{\omega-s_{14'}}\right)\end{aligned}\tag{3.23}$$

Where the spectrum density $\rho_J(\omega)\equiv\text{Im}b_J(\omega)$, $s_{14'}=(p_1-p_{4'})^2$, and $s_0=(4\mu^2+t)/2$ is the $s\leftrightarrow u$ symmetric point. The spectrum density is defined by the imaginary part of the amplitude, which equals the product of three-point tree amplitudes, the residue at the UV-mass pole.

$$\text{Im}\mathcal{B}_4(\omega,t)=16\pi\sum_{J=0}^{\infty}(2J+1)\rho_J(\omega)\mathcal{P}_J\left(1+\frac{2t}{\omega-4\mu^2}\right)=\pi\sum_{J=0}^{\infty}\delta_J(\omega)\mathcal{A}^1\mathcal{A}^4.\tag{3.24}$$

Here since the product of two three-point amplitudes has mass dimension 2, we denote the product of UV three-point tree amplitudes $\mathcal{A}^1\mathcal{A}^4=M_J^2\,h_J\big(1+2t/(\omega-4\mu^2)\big)$, where M_J^2 is the UV-mass encoded in the distribution $\delta_J(\omega)$. Plugging in the low-energy ansatz on the L.H.S. in Eq. (3.23), and performing a large ω expansion on the R.H.S.

$$\begin{aligned}&\because\ \mathcal{P}_J\big(\big(1+2t/(\omega-4\mu^2)\big)\big)=1+\mathcal{O}(t/\omega,\mu^2/\omega),\\ &\therefore\ h_J\big(1+2t/(\omega-4\mu^2)\big)=h_J^{(0)}+\mathcal{O}\left(1/\omega\right),\quad C_2=2\sum_{J=0}^{\infty}\int_{\Lambda^2}^{\infty}\frac{dM_J^2}{M_J^4}\delta_J(M_J^2)\,h_J^{(0)}.\end{aligned}\tag{3.25}$$

In the last line, we have replaced the integration variable ω with M_J^2 because the integral is evaluated against the distribution $\delta_J(\omega)$, whose support lies precisely at the UV mass poles M_J^2. Now, we can re-express the functions $f_J^{(2)}(z)$ and $g_J^{(2)}(z)$ in terms of $h_J^{(0)}$ under the triple cuts

$$f_J^{(2)}(z)=h_J^{(0)}\tilde{f}^{(0)}(z),\quad g_J^{(2)}=h_J^{(0)}\tilde{g}^{(0)}(z),\tag{3.26}$$

and let the Laurent series for $\tilde{f}^{(0)}(z)$, $\tilde{g}^{(0)}(z)$

$$\tilde{f}^{(0)}(z)=\cdots\tilde{f}_{-1}/z+\tilde{f}_0+\tilde{f}_1z+\cdots,\quad \tilde{g}^{(0)}(z)=\cdots\tilde{g}_{-1}/z+\tilde{g}_0+\tilde{g}_1z+\cdots\tag{3.27}$$

The *leading* anomalous threshold contribution in Eq. (3.19)

$$\begin{aligned}\Delta B^{+-}_{2,\text{UV anom}}=2\pi iC_2\Bigg[&\left(\int_{\zeta_\triangleright^+}^{\zeta_\triangleright^-}+\int_{\zeta_\triangleleft^+}^{\zeta_\triangleleft^-}\right)\frac{d\zeta}{\zeta^3}\frac{\left(\tilde{f}^{(0)}(z_+^0)+\tilde{f}^{(0)}(z_-^0)\right)}{2(s_2-s_3)}\\ &+\int_{\zeta_\triangleright^+}^{\zeta_\triangleright^-}\frac{d\zeta}{\zeta^4}\left(\frac{\tilde{f}_{-1}}{4\gamma q\cdot p_3}+\frac{\tilde{f}_1}{4\bar{q}\cdot p_3}\right)+\int_{\zeta_\triangleleft^+}^{\zeta_\triangleleft^-}\frac{d\zeta}{\zeta^4}\left(\frac{\tilde{g}_{-1}}{4\gamma' q'\cdot p_1}+\frac{\tilde{g}_1}{4\bar{q}'\cdot p_1}\right)\Bigg]\end{aligned}\tag{3.28}$$

The UV information has been packaged into the dimension-eight Wilson coefficients, as expected.

4 Application: SMEFT

In this section, we extend the analysis of anomalous thresholds to a more complicated example, the scattering process involving two down-quarks and two unstable Higgs.

4.1 SMEFT Setup

First, since the scattering process involves spinning particles, let's first discuss the amplitude basis and dispersion relation. Let external states 2 and 3 be the unstable Higgs bosons, with spin-0, and 1 and 4 be the right-handed down-quarks, with spin-$1/2$.

Scattering Amplitude: Independent Helicity Spinor Product Basis

The S-matrix element with external spinning states can be decomposed into the scalar component $\mathcal{A}_{4,k}(s,t)$, which is Lorentz-invariant, and the tensor component $\mathbf{A}_k(I_1,I_4)$, which reflects the Lorentz transformation of external states. Note that the tensor components can be written in terms of massive helicity spinors. Consider a four-point amplitude with external states 1 and 4 having spin-$1/2$, where $I_1,\ I_4{=}1,2$ denote their little group indices.

$$\mathcal{A}_4(p_i,I_1,I_4){=}\sum_k A_{4,k}(s,t)\mathbf{A}_k(I_1,I_4), \tag{4.1}$$

$$\mathbf{A}_k(I_1,I_4){=}\langle\mathbf{14}\rangle^{a_k}[\mathbf{14}]^{b_k}\langle\mathbf{1}p_i\mathbf{4}]^{c_k}\langle\mathbf{1}p_ip_j\mathbf{4}\rangle^{d_k}[\mathbf{1}p_ip_j\mathbf{4}]^{e_k} \tag{4.2}$$

Here the parameters $a_k,\ b_k,\ c_k,\ d_k,\ e_k$ are determined by the spins of the external states $\mathbf{A}_k(I_1,I_4)\propto\lambda_1^{I_1}\lambda_4^{I_4}$, and the little group indices are suppressed in the above expression. In this case, the angle or square bracket of external states 1 and 4 can only appear once in the tensor components. All linear-independent tensor components are listed in below:

$$\mathbf{A}_k(I_1,I_4){=}\langle\mathbf{14}\rangle,\ [\mathbf{14}],\ \langle\mathbf{1}p_{23}\mathbf{4}],\ \langle\mathbf{1}p_2p_3\mathbf{4}\rangle,\ [\mathbf{1}p_2p_3\mathbf{4}]. \tag{4.3}$$

Here $p_{23}{=}p_2{-}p_3$ and we have used on-shell condition, momentum conservation, and gamma-matrices algebra to find the linear-independent tensor components, and note that here we do not take the right-handedness of down-quarks. The general on-shell amplitude with scalars s and fermions f is

$$\mathcal{A}(f{+}s{\to}f{+}s){=}\mathcal{A}_{4,1}\langle\mathbf{14}\rangle{+}\mathcal{A}_{4,2}[\mathbf{14}]{+}\mathcal{A}_{4,3}\langle\mathbf{1}p_{23}\mathbf{4}]{+}\mathcal{A}_{4,4}\langle\mathbf{1}p_2p_3\mathbf{4}\rangle{+}\mathcal{A}_{4,5}[\mathbf{1}p_2p_3\mathbf{4}] \tag{4.4}$$

Note that in the view of dispersion relation, however, the tensor components should not be viewed independent to the scalar components, and this is because the helicity spinor products can be expressed in terms of Mandelstam variable s and t. A quick way to obtain the helicity spinor products in terms of s and t is by picking the centre of mass (C.O.M.) frame, since we are considering elastic scattering

$$p_1^\mu{=}(E,0,0,p),\quad p_2^\mu{=}(E',-\mathbf{p}_1),\quad p_4^\mu{=}(E,p\sin\theta,0,p\cos\theta),\quad p_3^\mu{=}(E',-\mathbf{p}_4). \tag{4.5}$$

Here $E{=}\sqrt{p^2{+}m^2}$, $E'{=}\sqrt{p^2{+}M_R^2}$, and the corresponding helicity spinors

$$\lambda_\beta^{\ I_1}(1){=}\tilde{\lambda}_{I_1\dot{\beta}}(1){=}\frac{1}{\sqrt{2(m{+}E)}}\begin{pmatrix}m{+}E{+}p & 0\\ 0 & m{+}E{-}p\end{pmatrix}, \tag{4.6}$$

$$\lambda_\beta^{\ I_4}(4){=}\tilde{\lambda}_{I_4\dot{\beta}}(4){=}\frac{1}{\sqrt{2(m{+}E)}}\begin{pmatrix}m{+}E{+}p\cos\theta & p\sin\theta\\ p\sin\theta & m{+}E{-}p\cos\theta\end{pmatrix}. \tag{4.7}$$

The relation between the kinematics in C.O.M. (energy and scattering angle) and Mandelstam variables

$$E=\frac{s+m^2-M_R^2}{2\sqrt{s}},\quad E'=\frac{s-m^2+M_R^2}{2\sqrt{s}},\quad p=\frac{\mathcal{F}(s)}{2\sqrt{s}},\quad \cos\theta=\frac{s(t-u)+(m^2-M_R^2)^2}{\mathcal{F}(s)^2}.$$

Here $\mathcal{F}(s)\equiv\sqrt{(s-(m-M_R)^2)\,(s-(m+M_R)^2)}$. Thus, one can compute the helicity spinor product in the C.O.M. first, and then utilize these relations to express them covariantly. For instance, $\langle\mathbf{1}^1\mathbf{4}^1\rangle=-(m+E+p)p\sin\theta/\,(2(m+E))\to-\sqrt{t(s+t)/s}$ as $m, M_R\to 0$. In this sense, we find that the tensor components are proportional to $\sqrt{t}$ except $\langle\mathbf{1}p_{23}\mathbf{4}]$; therefore, under the forward limit $\theta\to 0$, the amplitude becomes

$$\mathcal{A}(f+s\to f+s)\to\mathcal{A}_{4,3}(s,0)\langle\mathbf{1}p_{23}\mathbf{4}]$$

Since the high-energy behavior $s\to\infty$ of the tensor component $\langle\mathbf{1}p_{23}\mathbf{4}]\to s$, we take the once-subtracted dispersion on the scalar component

$$B_2(f+s\to f+s)\equiv\int\frac{ds'}{2\pi i}\frac{\mathrm{Disc}_s\mathcal{A}_{4,3}(s')}{(s'-s_0)^2}.\tag{4.8}$$

4.2 Violation of Positivity

Next, let's introduce two full theories where UV fields are minimally coupled to the down-quark field. Consider renormalizable BSM theories that involve a UV massive scalar doublet, denoted as Ψ, or a UV massive vector singlet, referred to as $\mathbf{A}_\mu$[5]. These UV fields are minimally coupled to a pair of down-type quarks, specifically $\bar{Q}^a_{L,i}$ and d^a_R, where $\{a,b,c,\cdots\}$ denotes the SU(3) gauge group indices and $\{i,j,k,\cdots\}$ denotes the SU(2) gauge group indices[6]. For the down quark fields with definite handedness to consistently couple to the UV scalar field, it has to be a SU(2) scalar doublet,

$$\mathcal{L}_{\text{full},0}=\mathcal{L}_{\text{SM}}+(D^\mu\Psi_i)^\dagger D_\mu\Psi_i-m^2_{\text{UV}}\Psi_i^\dagger\Psi_i-y\bar{Q}_{L,i\,a}\Psi_i d^a_R-y^*\bar{d}_{R,a}\Psi_i^\dagger Q^a_{L,i}.\tag{4.9}$$

Here

$$Q^a_{L,i}=\begin{pmatrix}u_L\\ d_L\end{pmatrix},\quad \Psi_i=\begin{pmatrix}\psi^+\\ \psi^0\end{pmatrix},\quad \Psi_i^\dagger=\begin{pmatrix}\psi^-&\psi^{0*}\end{pmatrix},$$

$\psi^-\equiv\psi^+$ and the Yukawa coupling y is real.

On the other hand, the down quark fields can consistently couple to the UV vector singlet, and the renormalizable theory with massive vectors can be constructed via the Stueckelberg mechanism.

$$\begin{aligned}\mathcal{L}_{\text{full},1}=\mathcal{L}_{\text{SM}}&-\frac{1}{4}\mathbf{F}^2+\frac{m^2_{\text{UV}}}{2}\left(\mathbf{A}^\mu-\frac{1}{m_{\text{UV}}}\partial^\mu\mathbf{B}\right)^2-\frac{1}{2\alpha}(\partial\cdot\mathbf{A}+\alpha m_{\text{UV}}\mathbf{B})^2\\&+e\epsilon\bar{d}_{R,a}\not{\mathbf{A}}d^a_R+e\epsilon\bar{Q}^i_{L,a}\not{\mathbf{A}}Q^a_{L,i}+e\epsilon\bar{u}_{R,a}\not{\mathbf{A}}u^a_R.\end{aligned}\tag{4.10}$$

In the Lagrangian Eq. (4.10), the last term in the first line is gauge fixing with α being an arbitrary parameter, which is usually set to unity, and $\mathbf{B}$ is the Stueckelberg scalar field. In the following, let the masses of up-quark and down-quark $m_u=m_d=m$ and the hierarchy of scales $m^2_{\text{UV}}\gg s,t,s_i,m$

[5] We construct a renormalizable theory with massive vector fields using Stueckelberg's mechanism, as discussed in [9].

[6] For simplicity, we only consider one generation and two flavors (up and down) of quarks in the following discussion.

Scalar Doublet Case:

Let's compute the box diagrams in the BSM theory in Eq. (4.9), and evaluate the $s\langle \mathbf{1}p_{23}\mathbf{4}]$ coefficient in the large mass expansion. The one-loop Feynman diagrams relevant to this scattering process, with internal IR propagators being down-quarks, are

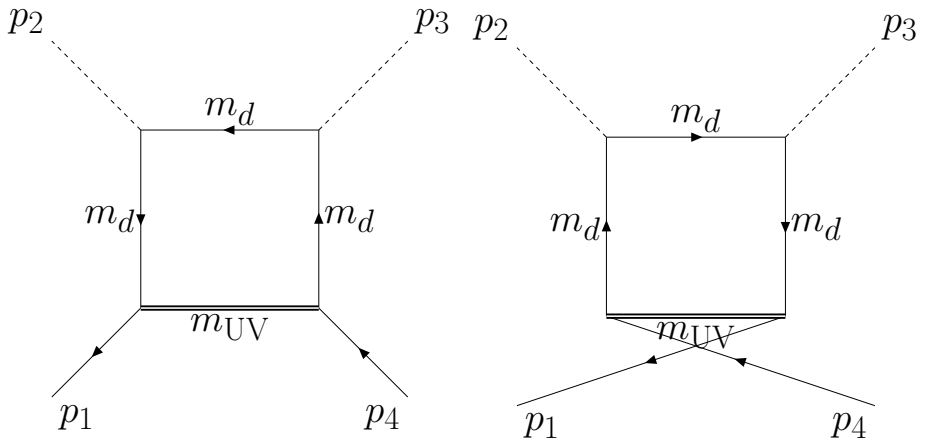

Figure 10: The s-channel and u-channel one-loop diagrams contributing to the scattering process at one-loop level. Here $m_d{=}m$.

$$\mathcal{I}_{\text{box},0}(D_R{+}h{\to}\bar{D}_R{+}h) = c_0 \int \frac{d^4L}{i\pi^2} \frac{N_0}{(L_1^2-m^2)(L_2^2-m^2)(L_3^2-m^2)(L^2-m_{\rm UV}^2)}. \tag{4.11}$$

where

$$c_0 = g_d^2 y^2, \;\; N_0 = (i)^3\, \bar{v}(4)\, P_L(\not{L}_3 + m)(\not{L}_2 + m)(\not{L}_1 + m) P_R\, u(1),$$

and $L_1 = L + p_1$, $L_2 = L + p_{12}$, $L_3 = L + p_{123}$. Because of the hierarchy $m_{\rm UV}^2 \gg m^2, s_i$, we can evaluate the integral by the method of [1, 10]. Explicitly, we introduce an artificial scale Λ that separates the loop momentum: $\int dL \to \int^\Lambda dL + \int_\Lambda dL$. Here Λ is chosen such that $\Lambda^2 \ll m_{\rm UV}^2$ and $\Lambda^2 \gg m^2, s_i$, and in the following, the first piece of the integral corresponds to the soft region, and the second piece of the integral corresponds to the hard region.

In the soft region, $m_{\rm UV} \gg |L|, |p_i|, m$, and we can expand the propagator

$$\frac{1}{L^2 - m_{\rm UV}^2} = -\frac{1}{m_{\rm UV}^2}\Big(1 + \frac{L^2}{m_{\rm UV}^2} + \cdots\Big)$$

The method-of-regions calculation is equivalent to the large mass expansion introduced in section 3.2. The divergence in the integral is *dimensional-regularized*, and it corresponds to UV divergence due to our artificial soft expansion. Because there is no divergence in the original full box integral, this UV divergence is expected to cancel with the IR divergence in the artificial hard expansion [10]. On the other hand, in the hard region, $m_{\rm UV} \sim |L| \gg |p_i|, m$, and we expand the propagator $1/((L+P_i)^2 - m^2)$, where $P_i = \sum_{j=1}^i p_j$

$$\frac{1}{(L+P_i)^2 - m^2} = \frac{1}{L^2} - \frac{2L\cdot P_i + P_i^2 - m^2}{(L^2)^2} + \frac{\big(2L\cdot P_i^2 + P_i^2 - m^2\big)^2}{(L^2)^3} + \cdots. \tag{4.12}$$

Under the forward limit, we have the $s\langle \mathbf{1}p_{23}\mathbf{4}]$ coefficient in the large mass expansion

$$\frac{16\pi^2 m_{\rm UV}^4}{c_0} B_{2,0} \approx \frac{\left(s_2-4m^2\right)\Lambda_{\rm bub}(s_2,m,m)-\left(s_3-4m^2\right)\Lambda_{\rm bub}(s_3,m,m)}{s_2-s_3} + \log\left(\frac{m_{\rm UV}^2}{m^2}\right)-1/2. \tag{4.13}$$

Where $\Lambda_{\rm bub}(s_3,m,m)=\frac{\sqrt{s_3(s_3-4m^2)}}{s_3}\log\left(\frac{\sqrt{s_3(s_3-4m^2)}+2m^2-s_3}{2m^2}\right)$.

Vector Singlet Case:

The computation of the one-loop box diagram involving a UV massive spin 1 particle is akin to that of the previous case, though the Feynman rules differ slightly. The one-loop box Feynman integral is,

$$\mathcal{I}_{\rm box,1}(D_R{+}h{\to}\bar{D}_R{+}h) = c_1\int\frac{d^4L}{i\pi^2}\frac{N_1}{(L_1^2-m^2)(L_2^2-m^2)(L_3^2-m^2)(L^2-m_{\rm UV}^2)}. \tag{4.14}$$

Where

$$c_1=\left(-i\frac{m}{v}\right)^2(ie\epsilon)^2,\quad N_1=-(i)^3\,\bar{v}(4)\,P_L\gamma^\mu\,(\not{L}_3+m)(\not{L}_2+m)(\not{L}_1+m)\,\gamma_\mu P_R\,u(1).$$

Under the forward limit, the coefficient $B_{2,1}^{(s)}$ is

$$\frac{16\pi^2 m_{\rm UV}^4}{c_1} B_{2,1} \approx 2\Big[\frac{\left(s_2-4m^2\right)\Lambda_{\rm bub}(s_2,m,m)-\left(s_3-4m^2\right)\Lambda_{\rm bub}(s_3,m,m)}{s_2-s_3} + \log\left(\frac{m_{\rm UV}^2}{m^2}\right)-1/2\Big]. \tag{4.15}$$

We found out that if the coupling constants are set to unity, the coefficient $B_{2,1}=2B_{2,0}$.

Numerical Plots

In this section, we set the hierarchy as $m=1, m_{\rm UV}=1000$, and consider the numerical plot of B_2 at the stable $s_2=s_3<4m^2$ and in the unstable region, the conjugate case $+-$: $s_3=M_R^2-iM_R\Gamma,\ s_2=s_3^*$, and the same case $++$: $s_2=s_3=M_R^2-iM_R\Gamma$, respectively. The discontinuity function of the bubble diagram has a branch cut in $z>4m^2$, which indicates the appearance of the anomalous threshold in the one-loop box diagram, and the analytically continued $\Lambda_{\rm bub}$ on the unphysical sheet is given by

$$\Lambda_{\rm bub}^{\pm}(z)={\rm pv}\,\Lambda_{\rm bub}(z)\pm 2\pi i\frac{\sqrt{z(z-4m^2)}}{z}\ \ ({\rm Re}(z)>4m^2,\,{\rm sgn}\,({\rm Im}(z))=\mp) \tag{4.16}$$

The decay width $\Gamma>0$ in Fig. 7a in the quark sector $h{\to}\bar{D}_R{+}D_R$ at tree level

$$\Gamma_{h\to\bar{D}D}=\frac{1}{8\pi}g_d^2 M_R\left(1-\frac{4m^2}{M_R^2}\right)^{3/2}\theta(M_R^2-4m^2) \tag{4.17}$$

In the following, we numerically plot the coefficient B_2 in the stable and unstable regions at the leading order.

Scalar Doublet Case:

In the stable region, $s_3 < 4m^2$ and we have $s_2 = s_3$; in the unstable region, they are analytically continued to the unstable poles. Define the real part of s_3 to be $M_R^2 = \text{Re}\, s_3$, at the leading order

$$\frac{16\pi^2 m_{\text{UV}}^4}{c_0} B_{2,0}^{\text{stable}} = \frac{\left(2m^2 + M_R^2\right) \Lambda_{\text{bub}}(M_R^2, m, m)}{M_R^2} + \log\left(\frac{m_{\text{UV}}^2}{m^2}\right) + \frac{4m^2}{M_R^2} - \frac{1}{2} \tag{4.18}$$

$$\frac{16\pi^2 m_{\text{UV}}^4}{y^2} B_{2,0}^{+-} = \log\left(\frac{m_{\text{UV}}^2}{m^2}\right) + \text{pv}\, \Lambda_{\text{bub}}(M_R^2) - 16\pi^2 - \frac{1}{2} \tag{4.19}$$

$$\begin{aligned}\frac{16\pi^2 m_{\text{UV}}^4}{c_0} B_{2,0}^{++} = &\frac{\left(2m^2 + (M_R^2 - iM_R\Gamma)\right) \Lambda_{\text{bub}}^{+}\left(M_R^2, m, m\right)}{M_R^2 - iM_R\Gamma} + \log\left(\frac{m_{\text{UV}}^2}{m^2}\right) \\ &+ \frac{4m^2}{M_R^2 - iM_R\Gamma} - \frac{1}{2}.\end{aligned} \tag{4.20}$$

Where $M_R^2 < 4m^2$ in the stable region and $M_R^2 > 4m^2$ in the unstable region. From the numerical plot, as shown in Fig. (11), it is obvious that the positivity bound of B_2^{+-} is violated due to the large negative contribution from the anomalous threshold.

Vector Singlet Case:

From Eq. (4.15), the leading $B_{2,1}$ is given below,

$$\frac{16\pi^2 m_{\text{UV}}^4}{c_1} B_{2,1}^{\text{stable}} = \frac{2\left(2m^2 + M_R^2\right) \Lambda_{\text{bub}}(M_R^2, m, m)}{M_R^2} + 2\log\left(\frac{m_{\text{UV}}^2}{m^2}\right) + \frac{8m^2}{M_R^2} - 1 \tag{4.21}$$

$$\frac{16\pi^2 m_{\text{UV}}^4}{(e\epsilon)^2} B_{2,1}^{+-} = 2\log\left(\frac{m_{\text{UV}}^2}{m^2}\right) + 2\text{pv}\, \Lambda_{\text{bub}}(M_R^2) - 32\pi^2 - 1 \tag{4.22}$$

$$\begin{aligned}\frac{16\pi^2 m_{\text{UV}}^4}{c_1} B_{2,1}^{++} = &\frac{2\left(2m^2 + M_R^2 - iM_R\Gamma\right) \Lambda_{\text{bub}}^{+}(M_R^2, m, m)}{M_R^2 - iM_R\Gamma} + 2\log\left(\frac{m_{\text{UV}}^2}{m^2}\right) \\ &+ \frac{8m^2}{M_R^2 - iM_R\Gamma} + 1\end{aligned} \tag{4.23}$$

Here $M_R^2 < 4m^2$ in the stable region and $M_R^2 > 4m^2$ in the unstable region.

In both cases, the anomalous-threshold contribution arises solely from the soft-region result, and this indicates that it can be computed within EFT. *The framework of the IR-computable anomalous-threshold contribution for more general cases is currently under construction.* We have introduced the IR-computable anomalous-threshold contribution for four-scalar scattering in section 3.3. Let the anomalous-threshold contribution be the additional term when the external kinematics are analytically continued to the unstable poles

$$\Delta B_{2,\text{UV anom}}^{+-} = \begin{cases} -16\pi, & \text{for UV scalar doublet} \\ -32\pi, & \text{for UV vector singlet.} \end{cases} \tag{4.24}$$

By subtracting this term $\Delta B_{2,\text{UV anom}}^{+-}$ in Eq. (4.20), the positivity is restored in the unstable region, as shown in Fig. 12.

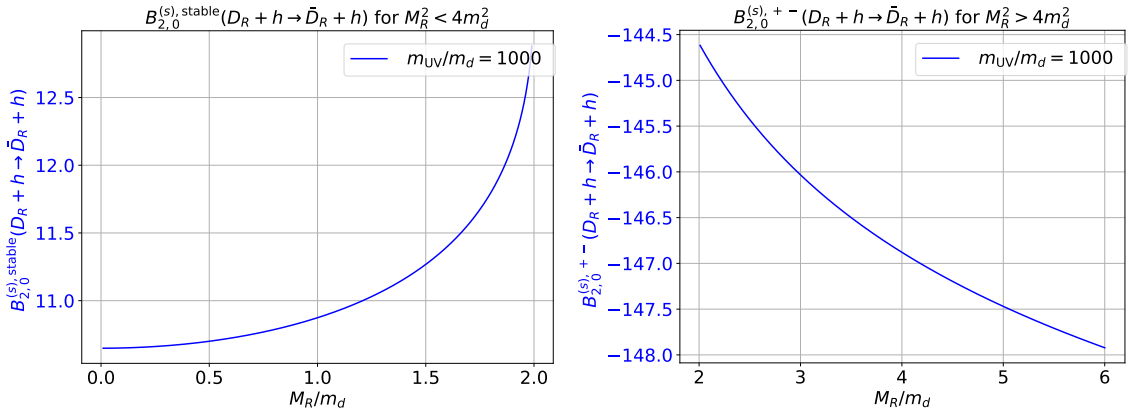

(a) $\frac{16\pi^2 m_{\mathrm{UV}}^4}{c_0} B_{2,0}^{\mathrm{stable}}$ (b) $\frac{16\pi^2 m_{\mathrm{UV}}^4}{y^2} B_{2,0}^{+-}$

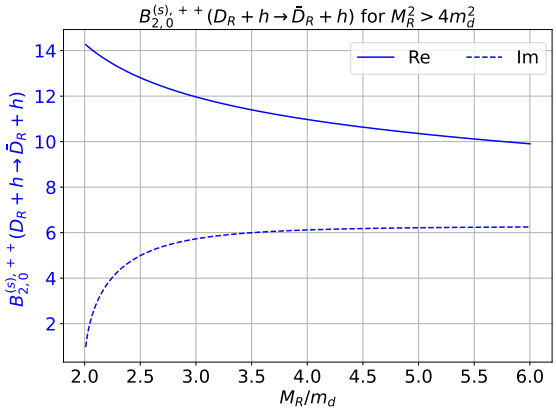

(c) $\frac{16\pi^2 m_{\mathrm{UV}}^4}{c_0} B_{2,0}^{(s),++}$

Figure 11: Normalized expansion coefficient B_2 in scalar double BSM theory, plotted in three figures due to the significant variation in range, particularly for $16\pi^2 m_{\mathrm{UV}}^4/y^2\, B_{2,0}^{\pm}$. The complex coefficient $16\pi^2 m_{\mathrm{UV}}^4/c_0\, B_{2,0}^{++}$ is represented with real and imaginary parts shown as solid and dashed lines, respectively. The coupling constant is set to $g_d = 1$ for illustration.

Acknowledgments

This manuscript serves as a research note for an ongoing collaboration. The author is deeply grateful for the guidance provided by Professor Katsuki Aoki and Professor Yu-tin Huang. Any errors or incomplete arguments that remain should be attributed solely to the author.

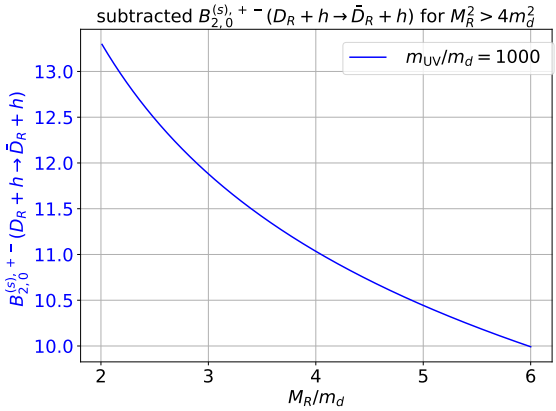

Figure 12: $B_2^{(s),+-}-\Delta B_2^{(s),+-}$, after subtracting the anomalous-threshold contribution, the positivity is restored in the unstable region.

A Conventions for Massive Helicity Spinor

In this section, we introduce the convention of the massive helicity spinor [11] used in this paper. Let's start by introducing the massive helicity spinor variables.

$$\not{p} \equiv p^\mu \gamma_\mu = \begin{pmatrix} 0 & p_{\alpha\dot{\beta}} \\ p^{\dot{\alpha}\beta} & 0 \end{pmatrix}. \tag{A.1}$$

Which is a 4×4 matrix, and the on-shell condition $\not{p}\not{p} = m^2 \cdot \mathbb{1} \neq 0$ tells us that $p_{\alpha\dot{\beta}}\, p^{\dot{\beta}\delta} = m^2\, \delta_\alpha^\delta$, which means $p_{\alpha\dot{\beta}}$ and $p^{\dot{\alpha}\beta}$ are rank-2 tensor with determinant m, and can be written as the sum of two rank-one tensors, whose determinants are $e^{\pm i\theta}m$

$$p_{\alpha\dot{\alpha}} = \lambda_\alpha^I \tilde{\lambda}_{\dot{\alpha} I} = \epsilon_{IJ}\lambda_\alpha^I \tilde{\lambda}_{\dot{\alpha}}^J. \tag{A.2}$$

Where I is called the little group indices, and this corresponds to the fact that there is an ambiguity of choice of $\lambda, \tilde{\lambda}$ that keeps the momentum p invariant. The indices of $\mathrm{SL}(2,\mathbb{C})$ (I) and $\mathrm{SU}(2)$ (α and $\dot{\alpha}$) are raised and lowered by $2d$ Levi Civita symbols $\epsilon_{IJ}, \epsilon_{\alpha\beta}$. The fermionic wavefunctions in usual QFT textbooks can be related to these helicity spinors, which are more fundamental elements to represent the on-shell amplitudes. In this paper, the consistent choice is

$$u^I(p) = \begin{pmatrix} \lambda_\alpha^I(p) \\ \tilde{\lambda}^{\dot{\alpha},I}(p) \end{pmatrix}, \bar{u}^I(p) = \begin{pmatrix} -\lambda^{\beta,I}(p) & \tilde{\lambda}_{\dot{\beta}}^I(p) \end{pmatrix} \tag{A.3}$$

$$v^I(p) = \begin{pmatrix} -\lambda_\alpha^I(p) \\ \tilde{\lambda}^{\dot{\alpha},I}(p) \end{pmatrix}, \bar{v}(p) = \begin{pmatrix} \lambda^{\beta,I}(p) & -\tilde{\lambda}_{\dot{\beta}}^I(p) \end{pmatrix} \tag{A.4}$$

Once the helicity spinor variables satisfy the on-shell conditions

$$\begin{aligned} p_{\alpha\dot{\alpha}}\tilde{\lambda}^{\dot{\alpha},I} = m\lambda_\alpha^I, \;\; p_{\alpha\dot{\alpha}}\lambda^{\alpha,I} = -m\tilde{\lambda}_{\dot{\alpha}}^I \\ p^{\dot{\alpha}\alpha}\tilde{\lambda}_{\dot{\alpha}}^I = -m\lambda^{\alpha,I}, \;\; p^{\dot{\alpha}\alpha}\lambda_\alpha^I = m\tilde{\lambda}^{\dot{\alpha},I}. \end{aligned} \tag{A.5}$$

Just as the massless helicity spinor, we usually use the angle and the square brackets as well as $\lambda, \tilde{\lambda}$ interchangeably, where $|p] \equiv \lambda_\alpha^I$ and $|p\rangle \equiv \tilde{\lambda}^{\dot{\alpha},I}$. The angle and square bracket are connected through the on-shell condition. Our goal is to find the linearly independent helicity spinor products for 2-2 scattering, and therefore we restrict the basis to at most one momentum insertion between brackets. Note that the massive helicity spinors are eigenstates of the chiral projectors, $P_L \equiv 1/2(1-\gamma_5), P_R \equiv 1/2(1+\gamma_5)$,

$$P_{L,\beta}^{\alpha}\lambda_\alpha^I = \lambda_\beta^I, \quad P_{R,\dot{\alpha}}^{\dot{\beta}}\tilde{\lambda}^{I,\dot{\alpha}} = \tilde{\lambda}^{I,\dot{\beta}} \tag{A.6}$$

It is crucial because the Standard Model is chiral.

References

[1] K. Aoki and Y.-t. Huang, *Anomalous thresholds for the S-matrix of unstable particles*, *JHEP* **09** (2024) 045 [2312.13520].

[2] W. Lucha, D. Melikhov and S. Simula, *Dispersion representations and anomalous singularities of the triangle diagram*, *Phys. Rev. D* **75** (2007) 016001 [hep-ph/0610330].

[3] K. Aoki, *Unitarity and unstable-particle scattering amplitudes*, *Phys. Rev. D* **107** (2023) 065017 [2212.05670].

[4] D. Forde, *Direct extraction of one-loop integral coefficients*, *Phys. Rev. D* **75** (2007) 125019 [0704.1835].

[5] Z. Bern, L. Dixon and D. Kosower, *Dimensionally regulated one-loop integrals and the unitarity method*, *Phys. Lett. B* **302** (1993) 299 [hep-ph/9212308].

[6] Z. Bern, L. Dixon and D. Kosower, *One-loop corrections to five-gluon amplitudes*, *Nucl. Phys. B* **425** (1994) 217 [hep-ph/9403226].

[7] Z. Bern, L. Dixon and D. Kosower, *Progress in one-loop QCD computations*, *Ann. Rev. Nucl. Part. Sci.* **46** (1996) 109 [hep-ph/9602280].

[8] G. Passarino and M.J.G. Veltman, *One Loop Corrections for e+ e- Annihilation Into mu+ mu- in the Weinberg Model*, *Nucl. Phys. B* **160** (1979) 151.

[9] M. Fabbrichesi, E. Gabrielli and G. Lanfranchi, *The Dark Photon*, 2005.01515.

[10] A.V. Manohar, *Introduction to Effective Field Theories*, 1804.05863.

[11] N. Arkani-Hamed, T.-C. Huang and Y.-t. Huang, *Scattering amplitudes for all masses and spins*, *JHEP* **11** (2021) 070 [1709.04891].